ELSEVIER

Marine and Petroleum Geology 20 (2003) 459–470

Marine and Petroleum Geology

www.elsevier.com/locate/marpetgeo

Predictions of gas hydrate phase equilibria and amounts in natural sediment porous media

Jeffery B. Klauda, Stanley I. Sandler*

Department of Chemical Engineering, Center for Molecular and Engineering Thermodynamics, University of Delaware, Newark, DE 19716, USA

Received 12 August 2002; received in revised form 10 May 2003; accepted 15 May 2003

Abstract

Hydrates in marine sediments are estimated to contain more methane than conventional reserves. Previous estimates of the amounts of methane hydrate ignore pore size effects and variations in hydrate saturation of the pore space. The model presented here uses sediment type, geothermal gradient, and seafloor depths as inputs, and leads to predictions for the maximum depth of hydrate stability for data collected in the Ocean Drilling Program with an average error of 5%. Reaction-mass transfer partial differential equations are solved to estimate the amount of hydrate filling of the pore space, rather than using previous ad hoc choices for hydrate saturation. Predictions for the amounts of methane hydrate in the Mediterranean Sea, the Black Sea, the Gulf of Mexico, and the Northern Indian Ocean are made.

Keywords: Gas hydrates; Clathrates; Porous media

1. Introduction

Gas hydrates or clathrates are crystalline compounds that form from water with at least one other compound, and are stable at conditions above the normal freezing point of water. Methane is one of many guests that can form hydrates and will be considered here because of its abundance in the ocean seafloor regions where large masses of hydrates exist. There has been interest in developing methods to harvest the huge amounts of methane present in natural gas hydrates. A recent estimate of the amount of methane trapped in hydrates is as much as 300 times that in conventional US reserves (Sloan, 1998). Also, the melting and dissociation of gas hydrates in the ocean floor and in permafrost regions might increase global warming (Hatzikiriakos & Englezos, 1993; Hatzikiriakos & Englezos, 1994) resulting in further hydrate dissociation. Conversely, sequestering of carbon dioxide in hydrates has been proposed to reduce the amount of this greenhouse gas in the environment. Brewer, Friederich, Peltzer, and Orr (1999) and Brewer, Orr, Friederich, Kvenvolden, and Orange (1998) have experimentally shown the formation of CO_2 hydrates in the ocean.

Most measurements and models have been for bulk gas hydrates that are important in industrial pipelines, but for which capillary effects are unimportant. Methane hydrates in nature occur in porous media, e.g. clay, silt, and sand, where capillary forces (surface tension) can be important, and result in a hydrate equilibrium pressure that increases as the pore size decreases. Handa and Stupin (1992) first examined the effect of pore size on the equilibrium pressures of methane hydrates with laboratory prepared porous silica gel, and Uchida, Ebinuma, and Ishizaki (1999) measured the equilibrium pressures of methane hydrates in pores of different sizes. However, measurements of hydrate equilibrium pressures in natural porous media (clay, silt, or sand) in the laboratory are limited.

Seafloor hydrates are thermodynamically stable when at a given temperature the hydrostatic pressure is higher than the equilibrium pressure. However, the hydrate equilibrium pressure increases with depth due to increasing temperature as a result of the geothermal gradient. Therefore, there is a maximum depth of hydrate stability in the seafloor below which the hydrostatic pressure is less than the hydrate equilibrium pressure. Clennell, Hovland, Booth, Henry, and Winters (1999) and Henry, Thomas, and Clennell (1999)

* Corresponding author. Tel.: +1-302-831-2945; fax: +1-302-831-3226.
E-mail address: sandler@udel.edu (S.I. Sandler).

0264-8172/03/$ - see front matter © 2003 Elsevier Ltd. All rights reserved.
doi:10.1016/S0264-8172(03)00064-3

Nomenclature

a	activity
A	area
AAD	absolute average deviation
c	concentration
D	diffusion coefficient
E	methane expansion factor from hydrate to gas at STP
f	fugacity
h	hydrate saturation of pore space
L	length scale (2000 m)
mbsf	meters below sea floor
P	pressure
r	pore radius
$\Re_h$	rate constant for hydrate
R	gas constant
R_p	mean radius of the pore
sd	standard deviation of pore sizes
S	sedimentation rate
STP	standard temperature and pressure
t	time
T	temperature
u_f	fluid velocity
v_s	sediment velocity
vdWP	van der Waals and Platteeuw
$\underline{V}$	volume
x	molar composition in Liquid phase
x_{clay}	fraction of clay in sediment
y	depth below seafloor
z	scaled radius
Δz	equivalent thickness of pure hydrate in sediment

Greek characters

α	mass fraction of organic carbon
Δ	change in a property
ζ	shape factor
φ	probability distribution function
γ	activity coefficient
κ	conductivity
λ	rate constant for methanogenesis
μ	chemical potential
Φ	porosity
ρ	density
τ	temperature scale (10 °C)
θ	contact angle
σ	surface tension

Superscripts and subscripts

bulk	bulk phase
eq	equilibrium
f	fluid
hydro	hydrostatic
H	hydrate phase
L	liquid water
m	methane
s	sediment
sat	saturated conditions
V	vapor phase
w	water
ws	wet sediment
α	ice phase
β	empty hydrate phase
π	ice or liquid water

adapted the bulk hydrate model originally developed by van der Waals and Platteeuw (1959) to include the effect of surface tension on hydrates confined in pores. However, with their model, predictions for the maximum depths of methane hydrate stability differed significantly from those observed from the Ocean Drilling Program (ODP) Leg 164 (Paull et al., 1996).

The model we present here extends our recently developed fugacity-based model to predict bulk hydrate equilibrium pressures in pure water (Klauda & Sandler, 2000) to hydrates formed in natural porous media and from seawater. This model includes the effect of a distribution of pore sizes, and, as we show, leads to an accurate prediction for depths of hydrate stability in the seafloor. Our estimates for the amount of methane hydrate in several regions of the world are based on this thermodynamic model to determine the thickness of the hydrate stability zones and a mass transfer model of Davie and Buffett (2001) to estimate the amount of hydrate saturation of the sediment pore space.

2. Modeling hydrate equilibrium

The first model to predict bulk hydrate equilibrium was developed from statistical mechanics by van der Waals and Platteeuw (1959, vdWP) and extended by Parrish and Prausnitz (1972) to account for multiple guests in hydrate structures. Details of these models can be found in Sloan (1998). Recently, we have developed a somewhat different, classical thermodynamic approach to modeling gas hydrates, which has led to improved hydrate phase behavior predictions (Klauda & Sandler, 2000) for bulk single-guest hydrates. However, natural hydrates form in porous media, e.g. clayey sediments, so that capillary effects can be important. Also natural porous media have pores of varying sizes; in some locations the pore size distribution (PSD) can be quite narrow, while in others it is broad (Clennell et al., 1999). Extensions of the vdWP type models to hydrates formed in laboratory porous media (Clarke, Pooladi-Darvish, & Bishnoi, 1999) and in marine sediments (Henry et al., 1999) have used a single

pore size to determine the capillary effect on hydrate equilibrium pressures. We have found that extending our fugacity-based model to hydrates formed in silica gel with a distribution of pore sizes improved upon single pore size and vdWP type model predictions (Klauda & Sandler, 2001). Therefore, a model of hydrate formation in porous media should include a PSD when such information is available.

The equality of fugacity phase equilibrium condition was used in our model (Klauda & Sandler, 2000)

$$f_w^H(T,P) = f_w^\pi(T,P) \tag{1}$$

where $f_w^\pi(T,P)$ is the fugacity of water in the liquid ($\pi = L$) or solid ice ($\pi = \alpha$) phase, and the fugacity of water in the bulk hydrate phase is

$$f_w^H(T,P) = f_w^\beta(T,P)\exp\left(\frac{-\Delta\mu_w^H(T,P)}{RT}\right) \tag{2}$$

Here $f_w^\beta(T,P)$ is the fugacity of the hypothetical empty hydrate lattice and $\Delta\mu_w^H(T,P)$ is the difference in the chemical potential between the empty and filled hydrate lattice. The details and parameters used for this model, and especially the calculation of the fugacities $f_w^\beta(T,P)$ and $f_w^\pi(T,P)$ can be found elsewhere (Klauda & Sandler, 2000).

At temperatures above the normal freezing point of water, methane hydrate can develop from dissolved methane (Fig. 1(a)) in the aqueous phase (that is, without free gas), but usually there is gaseous methane present (Clennell et al., 1999). Since the interfacial tension between gaseous methane and liquid water is almost twice that of the ice-water interface, methane gas will preferentially fill the larger pores (Fig. 1(b)). Consequently, hydrate crystallization in pores will occur in direct contact with a continuous water phase, forming a granule of hydrate in the pore space (Fig. 1). It is assumed that on crystallization, the hydrate progressively protrudes into the pore space with a convex spherical cap. Therefore, for a pore with a radius of r the pressure in the hydrate phase, $P_{pore}^H(r)$, is higher than

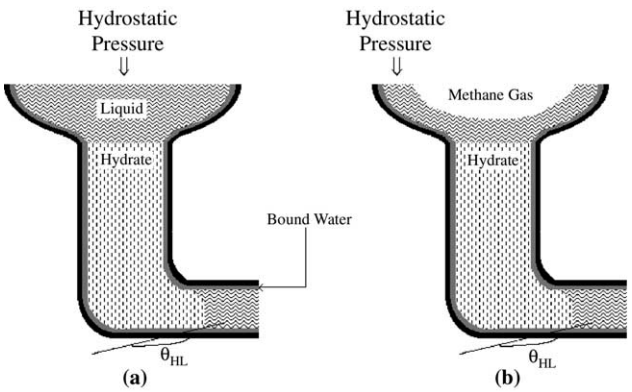

Fig. 1. Schematic of water interfaces in natural porous media.

the hydrostatic pressure in the bulk, P_{hydro}

$$P_{pore}^H(r) = P_{hydro} - \frac{\zeta_{HL}\sigma_{HL}}{r}\cos\theta_{HL} \tag{3}$$

where ζ is the shape factor, σ is the surface tension, and θ is the contact angle of the hydrate-liquid water (HL) interface, which is greater than 90° since the contact surface is convex. This differs from the formation of hydrates in artificial porous media (Handa & Stupin, 1992; Uchida et al., 1999) where the liquid water phase is discontinuous from the bulk. That is, the pressure on the water is not equal to the bulk pressure of the surrounding gas. For this situation the hydrate forms initially in pores open to the bulk gas phase, and then protrudes inwardly through the porous media (Klauda & Sandler, 2001), thereby affecting the pressure of the liquid water phase rather than the hydrate phase.

There has been no experimental determination of the surface tension between liquid water and hydrate; it will be assumed here to be equal to the ice-water surface tension of 27 mJ m^{-2} (Clennell et al., 1999; Handa & Stupin, 1992). Since there is a distribution of pore sizes in natural marine sediment, the average pressure in the hydrate phase is

$$\bar{P}_{pore}(r) = P_{hydro} - \int_0^\infty \frac{\zeta_{HL}\sigma_{HL}}{r}\cos\theta_{HL}\varphi(r)dr \tag{4}$$

where $\varphi(r)$ is the probability distribution function for pore size, which is assumed to be a normal distribution in our calculations

$$\varphi(r) = \frac{1}{\sqrt{2\pi}}\exp\left(\frac{(r-R_p)^2}{2\,sd^2}\right), \qquad z = \frac{r-R_p}{sd} \tag{5}$$

where R_p is the mean pore radius, sd is the pore size standard deviation, and z is the scaled radial distance.

A simple adaptation of our fugacity-based model (Klauda & Sandler, 2000) can be used to predict hydrate formation in natural porous media by assuming that the increase in pressure of the confined hydrate phase is accounted for by a Poynting correction to the fugacity

$$f_w^H(T,P_{hydro}) = f_w^{H,bulk}(T,P_{hydro})a_w^{HL}(T) = f_w^{H,bulk}(T,P_{hydro}) \times \exp\left[-\frac{\underline{V}_w^H(T,P_{hydro})(P_{hydro}-P_w^{sat,\beta}(T))}{RT}\right] \times \int_{-R_p/sd}^\infty a_w^{HL}(T,z)\varphi(z)dz \tag{6}$$

with

$$a_w^{HL}(T,z) = \exp\left[-\frac{\underline{V}_w^H}{RT}\frac{\zeta_{HL}\sigma_{HL}}{R_p - sd\,z}\cos\theta_{HL}\right] \tag{7}$$

where $f_w^{H,bulk}(T,P_{hydro})$ is the fugacity of water in the bulk hydrate, Eq. (2). Since it is assumed that the hydrate in a pore has a convex spherical cap, the shape factor, ζ_{HL}, is equal to two. The lower integration limit in Eq. (6), $-R_p/sd$, results from the physical limitation of positive pore radii.

Since the hydrate phase forms a convex shape in the pore, the contact angle for hydrate is assumed to be 180° (Fig. 1).

The fugacity of liquid water is modeled by

$$f_w^L(T,P_{hydro}) = x_w(T,P_{hydro})\gamma_w(x_w,T)P_w^{sat,L} \times \exp\left[\frac{V_w^L(T,P_{hydro})(P_{hydro}-P_w^{sat,L}(T))}{RT}\right] \quad (8)$$

where the composition of water, x_w, is determined from the solubility of methane in water computed using Henry's Law with constants for seawater (Cramer, 1984) and using the known concentration of electrolytes in seawater (Lide & Frederiskse, 1995). The activity of water in seawater was described using the Pitzer model for a single electrolyte in solution (Pitzer & Mayorga, 1973) and its extension to a mixed electrolyte solution by Patwardhan and Kumar (1986), where the seawater ion concentrations were obtained from the CRC Handbook (Lide & Frederiskse, 1995). Therefore, the equilibrium pressure at a specified temperature is determined by substituting Eqs. (6) and (8) into Eq. (1) and iteratively solving for the pressure.

3. Hydrate formation in nature

The necessary criteria for a methane hydrate to form in nature are: a sufficient amount of methane or organic matter and methane producing bacteria, and that the actual or hydrostatic pressure is greater than or equal to the methane hydrate equilibrium pressure. The first criterion can be satisfied by direct observation of hydrate occurrence from well logs, or indirect determinations of a free methane gas zone using seismic seafloor data to locate a region of strong reflections of sound waves (referred to as a bottom-simulating reflector or BSR) above which hydrates are stable. From ocean drilling data, the depth of the BSR corresponds closely to the deepest occurrence of hydrate in the seafloor (Paull et al., 1996). Therefore, the BSR is generally taken to represent the base of hydrate stability (Ruppel, 1997), and below which the hydrostatic pressure is less than the hydrate equilibrium pressure (due to the increasing temperature as a result of the geothermal gradient).

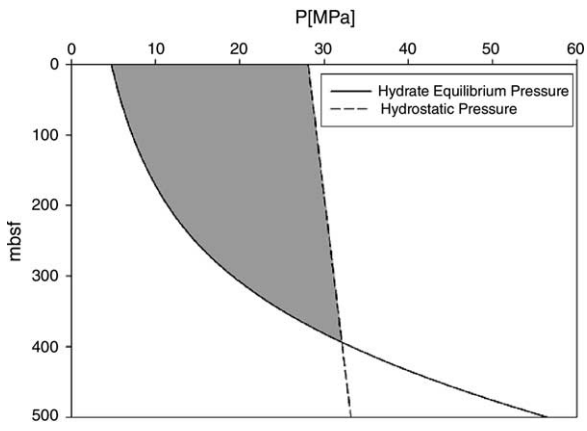

Fig. 2. Schematic of hydrate thermodynamic stability zone: shaded in gray.

The zone of hydrate stability is determined by comparing the hydrostatic pressure and equilibrium pressure at each depth below the seafloor. The hydrate phase is thermodynamically stable if the hydrostatic pressure is greater than or equal to the hydrate equilibrium pressure, as shown by the shaded gray region in Fig. 2. Thermodynamics cannot give us information on the amount of hydrate in this stability zone, though the available sediment pore space provides an upper bound to the volume available for hydrate growth. Later we will discuss how we estimate the percentage of the pore space filled by the hydrate using a previously developed set of mass transfer equations (Davie & Buffett, 2001).

3.1. Model parameters to determine hydrate zone thickness

The geothermal gradient, seafloor temperature and depth, and pore distribution are needed to predict the equilibrium pressures of the hydrate at a given depth below the seafloor and thereby the methane hydrate stability zone in the seafloor. The hydrostatic pressure is determined based on the density of seawater and the sum of the seafloor depth below sea level and the depth below seafloor, and compared with the equilibrium hydrate pressure to establish if the hydrate is thermodynamically stable.

3.1.1. Geothermal gradient

The geothermal gradient is essential in determining the temperature profile in the ocean sediment. A large geothermal gradient will produce a thin hydrate stability zone because of the steep increase in the ocean sediment temperature. Therefore, an accurate representation of the geothermal gradient is necessary. Previously Gornitz and Fung (1994) used an oceanic average for the geothermal gradient to estimate the amount of methane trapped in oceanic gas hydrates. However, in our calculations a region-specific geothermal gradient was used and obtained by interpolation of 19,807 global data points compiled by the International Heat Flow Commission (Gosnold, 2001; Pollack, Hurter, & Johnson, 1993).

3.1.2. Seafloor temperature and depth

The temperature at the ocean bottom compiled by in the 1998 World Ocean Atlas (Antonov et al., 1998a–c) varies between 1 and 5 °C at depths sufficient for hydrate stability. For the Indian Ocean a constant seafloor temperature of 1.5 °C has been used. However, for the inland seas and gulfs (Mediterranean Sea, Black Sea, and Gulf of Mexico) bottom water temperatures are typically higher than in the oceans. Therefore, the seafloor temperature in each inland sea was taken as an average value from those reported by Antonov et al. (1998a). The seafloor depth was obtained from high-resolution bathymetry data by Miller, Smith, Kuhn, and Sandwell (2000) and Smith and Sandwell (1997).

3.1.3. Pore size distribution

The pore size distribution (PSD) of the sediment is needed to accurately predict the hydrate stability zone in the seafloor. Soil and marine sediments can be considered to be of three general types: (1) clay—the finest of all sediments resulting in the smallest pores, (2) silt—coarser than clay, and (3) sand and gravel—the coarsest of the sediments producing large pores. Dewhurst, Aplin, and Sarda (1999) and Dewhurst, Aplin, Sarda, and Yang (1998) measured the effect of consolidation pressure and sediment particle size on various physical properties of sediment. Mercury intrusion porosimetry was used on different London Clay samples to determine the PSD as a function of sediment type and pressure. They found that the mean pore size decreased with an increase of consolidation pressure and with the percentage of clay in the sample. A previous prediction of the PSD for marine sediment in a region of known methane hydrate occurrence (Henry et al., 1999) did not consider the effect of consolidation pressure on pore size. The mean pore size they measured at atmospheric conditions is expected to be larger than that at the bottom of the ocean, which may be why the predictions for the BSR by Henry et al. (1999) were deeper than the measured values.

Since sediment type is easily determined, we developed a correlation (Klauda & Sandler, 2001) for mean pore size as a function of consolidation pressure and percentage of clay in the sediment using the porosimetry data (differential intrusion volume as a function of pore radius) measured by Dewhurst et al. (1999, 1998)

$$\ln(R_p) = 15.4215 - 21.9773x_{clay} + 11.5670x_{clay}^2 + 0.2\,e^{(-0.0278P)} \quad [P \text{ in MPa and } R_p \text{ in Å}] \tag{9}$$

where x_{clay} is the fraction of clay-sized particles in the sediment sample. With this correlation a simple measuring technique, e.g. smear slides, can be used to estimate pore sizes instead of direct measurements. Here we have used values for the percentages of clay that were globally interpolated from 250 data points reported by the Deep Sea Drilling Project at methane hydrate stability depths below the seafloor (Musich et al., 2000).

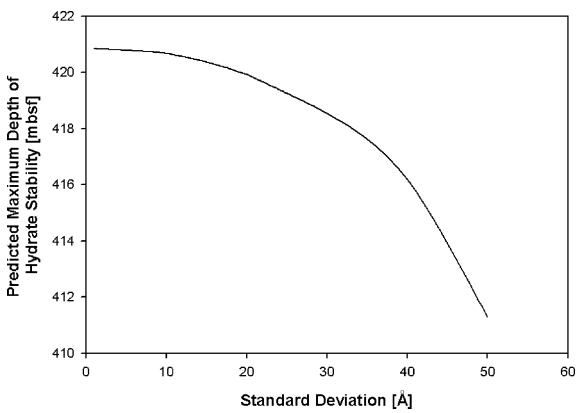

Fig. 3. Predicted maximum depth of hydrate stability or BSR as a function of the standard deviation in pore size distribution for site 994 of ODP Leg 164.

The standard deviation of the fitted normal distribution decreased with increasing pressure, but there was no evident dependency on the fraction of clay. We have found that the effect of the PSD is important near the depressed freezing point in artificial porous media, because of the variation in the freezing point of water with pore size (Klauda & Sandler, 2001). However, the effect of the PSD on the predicted equilibrium pressures at temperatures higher than the freezing point is less. The geological properties at Site 994 of ODP Leg 164 (Paull et al., 1996) are used in Fig. 3 to show the effect of the pore size standard deviation on the predicted maximum depth of hydrate stability. For the range of standard deviations considered, there is less than a 10 m decrease in the maximum depth of hydrate stability. The porosimetry measurements of Dewhurst et al. (1998, 1999) showed a range of standard deviations from about 10 to 30 Å. A constant standard deviation of 20 Å was used here for all sediment types.

3.2. Hydrate saturation of pore space

The degree of hydrate saturation in the pore space is crucial to accurately estimate the total quantity of methane hydrate. This factor has introduced a large uncertainty in previous calculations because of the ad hoc choice of hydrate saturation. In most estimates a globally constant hydrate saturation value between 5 and 10% of the pore space within the hydrate stability zone has been assumed (Gornitz & Fung, 1994; Kvenvolden & Grantz, 1990). However, hydrate saturation varies depending on the amount of methane available from the in situ production of methane from bacteria or from thermogenic sources from deep in the ocean floor. In the Blake Ridge Region, offshore of South Carolina, hydrate saturation varies from 2 to 7% of the pore space (Holbrook, Hoskins, Wood, Stephen, & Lizarralde, 1996), while at the Chile Triple Junction region, up to 18% of the pore space is filled with hydrate (Brown, Bangs, Froelich, & Kvenvolden, 1996).

Recently, Davie and Buffett (2001) developed a set of mass transfer equations for methane, organic carbon, chlorine, and hydrate that can be used to determine the pore space hydrate saturation profile. In this model hydrate growth is assumed to begin when the concentration of methane in water exceeds the equilibrium concentration in seawater and hydrate dissociates if the methane concentration is below the equilibrium value. The source of methane is assumed to be from methanogenic bacteria feeding on seafloor organic carbon. The partial differential equations for hydrate growth, organic carbon, and methane are

$$\Phi\frac{\partial h}{\partial t} + \nabla\cdot(\vec{v}_s\Phi h) = \Re_h(c_m - c_{eq}) \tag{10}$$

$$\frac{\partial \alpha}{\partial t} = -\vec{v}_s\cdot\nabla\alpha - \lambda\alpha \tag{11}$$

$$\Phi(1-h)\frac{\partial c_m}{\partial t} + \vec{u}_f \cdot \nabla c_m = \nabla \cdot [D_m \Phi(1-h)\nabla c_m] + (c_m - c_h)\Re_h(c_m - c_{eq}) + \left(\frac{16\rho_s(1-\Phi)}{30\rho_f}\right)\lambda\alpha \quad (12)$$

where h is the hydrate volume fraction, Φ is porosity, c_m is the methane concentration in liquid water, c_h is the methane concentration in the hydrate, α is the mass fraction of organic carbon, ρ_s is the sediment density, and ρ_f is the seawater density. The diffusivity of methane in seawater, D_m, and the rate constant for hydrate growth, $\Re_h$, were assumed to be constant at 10^{-9} m^2 s^{-1} and 10^{-8} s^{-1}, respectively. The sediment and fluid velocities are considered only for the z direction (the seafloor depth)

$$\vec{v}_s = \left(\frac{1-\Phi(0)}{1-\Phi(z)}\right)S\vec{z} \quad (13)$$

$$\vec{u}_f = (1-\Phi(0))\left[\frac{\Phi(L)}{1-\Phi(L)} - \frac{\Phi(z)h(z)}{1-\Phi(z)}\right]S\vec{z} \quad (14)$$

where S is the sedimentation rate. For the equilibrium methane concentration, c_{eq}, Davie and Buffett (2001) used an exponential decay from the methane concentration at the maximum depth of hydrate stability, $c_{eq}(T_{max})$

$$c_{eq}(T) = c_{eq}(T_{max})\exp[(T - T_{max})/\tau] \quad (15)$$

where τ is equal to 10 °C. Here $c_{eq}(T_{max})$ is determined from Henry's Law with the constants for seawater (Cramer, 1984). The initial conditions for methane concentration and hydrate volume were assumed to be zero. For organic carbon a steady state solution for Eq. (11) was used for the initial condition. The seafloor boundary conditions for methane concentration and hydrate volume were taken to be zero.

The parameters that have the most noticeable effect on the steady state solution of Eqs. (10)–(12) for hydrate saturation are the sedimentation rate, amount of available organic carbon at the seafloor, and rate constant for methanogenesis. However, the thickness of the hydrate zone, geothermal gradient, and seafloor porosity all affect the amount of hydrate in the pore space.

A steady state solution to the mass transfer partial differential equations is obtained between 1 and 10 Myr. The above-mentioned parameters may change during this time period. However, if we assume that the steady state solution is reached in the current time period, the initial conditions for these mass transfer equations are in the late Miocene and Pliocene Epochs, where most of the current continental margins were established. Climatic changes between ice ages and warm arid periods may also cause variations in these parameters, however, due to an inadequate understanding of such dependencies, the parameters will be assumed constant and equal to their current values.

The rate constant for methanogenesis from bacteria in ocean sediment, λ, is unknown, but Davie and Buffett (2001) determined a value of 3×10^{-13} s^{-1} to reproduce the salt water freshening for ODP Site 997 (Paull et al., 1996). However, this rate constant and the parameters given in Davie and Buffett (2001) lead to a prediction of the average hydrate saturation of 9% for the region between the BSR and 200 m above the BSR, which is higher than the 5–7% measured by Holbrook et al. (1996). Using the geological data for ODP Site 994, 995, and 997 (Paull et al., 1996) and the measured hydrate saturation (Holbrook et al., 1996), a value of λ was optimized to best fit the amount of hydrate saturation at steady state. We found that a value of 1.5×10^{-14} s^{-1} best correlates the hydrate saturation at ODP Leg 164, and assume that this is representative for the all regions we have considered.

The in situ microbial production of methane is largely constrained by the availability of organic carbon at the seafloor, and it is been reported that greater than 0.5% by weight of organic carbon is required (MacDonald, 1990; Revelle, 1983) for hydrate formation. The amount of organic carbon necessary to produce significant hydrate mass can be evaluated with the model of Davie and Buffett (2001). Fig. 4 is a contour plot of the predicted hydrate saturation as a function of sedimentation rate and percent organic carbon for $\lambda = 1.5 \times 10^{-14}$ s^{-1} and additional parameters taken from Davie and Buffett (2001). For sedimentation rates between 15 and 25 cm kyr^{-1} and 0.5% by weight of organic carbon on the seafloor, hydrate will, on average, fill from 0.5 to 1% of the pore space. At 0.4 wt% of organic carbon the hydrate pore space saturation is less than 0.5% for all sedimentation rates. Therefore, we considered areas of seafloor organic carbon of less than 0.4 wt% to have insufficient organic carbon to produce significant amounts of hydrate.

Fig. 4 also demonstrates the sensitivity of hydrate saturation of the pore space to the sedimentation rate. For example, with a seafloor organic content of 1% by weight, sedimentation rates of 50 and 15 cm kyr^{-1} result in 1 and

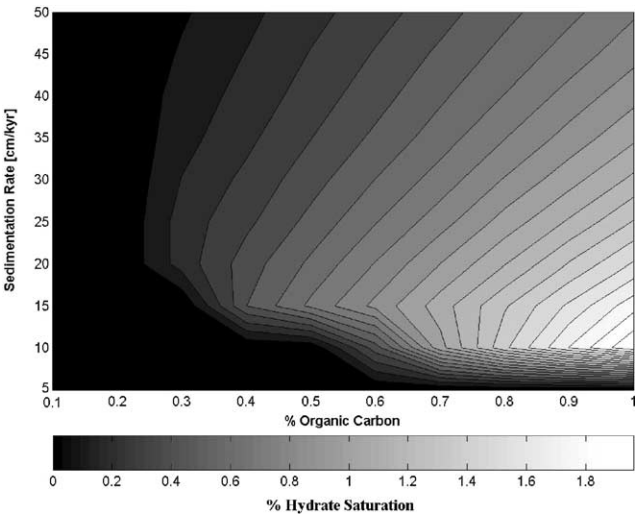

Fig. 4. Contour plot of the average percent hydrate saturation of the pore space in the hydrate thermodynamic stability zone.

2% hydrate saturation of the pore space, respectively. Sedimentation rates can vary significantly within a sea or ocean (Romankevich, 1984), but such data are sparse. Therefore, our assumption of an average sedimentation rate for each ocean or sea is appropriate given the limited available data. However, once more widespread sedimentation rate data become available, more accurate predictions of hydrate saturation of the pore space can be made.

The amount of organic carbon on the seafloor was interpolated from the data of Premuzic, Benkovitz, Gaffney, and Walsh (1982) and Romankevich (1984) for the regions considered here. Since the numerical data used in these references were not available, interpolation from their contour plots were used. The data of Romankevich (1984) was used for all locations except for the Gulf of Mexico, which were obtained from Premuzic et al. (1982).

The conductivity of wet sediment at the seafloor, κ_{ws}, at any point was interpolated from 15,529 global data points (Gosnold, 2001; Pollack et al., 1993) and indirectly used to predict the local porosity of the sediment at the seafloor, Φ_0, (Gornitz & Fung, 1994) using the geometric mean of the conductivity of water, κ_w, and dry sediment, κ_s

$$\kappa_{ws} = \kappa_w^{\Phi_0} \kappa_s^{(1-\Phi_0)} \tag{16}$$

where $\kappa_w = 0.57\ \mathrm{W\ m^{-1}\ K^{-1}}$ and $\kappa_s = 2.4\ \mathrm{W\ m^{-1}\ K^{-1}}$. The porosity as a function of the depth can be approximated by an exponential decay (Davie & Buffett, 2001; Gornitz & Fung, 1994)

$$\Phi(z) = \Phi_0 \exp(-z/L) \tag{17}$$

where z is the depth below the seafloor and L is the characteristic length scale for compaction assumed to be 2000 m.

3.3. Predicting locations and amount of methane hydrate

The amount of organic carbon on the seafloor and hydrate thermodynamic stability conditions determine whether a methane hydrate can form in given area. Here we will assume that methane comes from in situ production from bacteria and not from thermogenic methane production from deep in the seafloor, which we cannot determine. As stated above, 0.4 wt% of organic carbon is needed to produce a significant amount of hydrate, and we assume that values below this do not form hydrate.

The volume of methane at STP in methane hydrate is given by

$$V = AE \int_0^{\text{Base of Hydrate}} h(z)\Phi(z)\mathrm{d}z = AE\Delta z \tag{18}$$

where Δz is the equivalent hydrate zone thickness, $h(z)$ is the fraction of hydrate filling of the pore space solved from Eqs. (10)–(12), A is the aerial extent of the hydrate zone, and E is the gas expansion of methane from the hydrate to gas at STP. Since methane occupancy in the hydrate varies by only a few percent for the temperature and pressure ranges where hydrates form in the seafloor, E was set to 180 or 95% occupancy.

4. Results for local predictions of gas hydrate occurrences

4.1. BSR predictions

Estimating the maximum depth of hydrate stability without including the effect of pore size can lead to overpredictions by as much as 100 m (Klauda & Sandler, 2001) especially for clayey sediment. Our present predictions of the stability zone of hydrates in the seafloor are compared with measurements from the Ocean Drilling Project (ODP) (Behrmann et al., 1991; Paull et al., 1996; Westbrook et al., 1994) for seven drill sites with observed hydrates. The maximum depth of hydrate stability was measured indirectly by strong seismic reflection, BSR, which is taken to be the end of the hydrate zone and the beginning of the zone of free gas in the subsea sediment. Direct observations from ocean boreholes have also been used to determine the maximum depth of hydrate stability.

The percent differences between the measured base of hydrate and predictions from the fugacity model including porosity effects (sediment type) developed here are given in Table 1. In this table there are two predictions, one with

Table 1
Experimental and predicted baselines of hydrate stability in seafloor

ODP drilling site	%Clay near BSR	Water depth (m)	Base of hydrate (mbsf)	Measured error (m)	Predicted base[a] (mbsf)	%AD from measured[a]	Predicted base[b] (mbsf)	%AD from measured[b]
997	82.4	2770.1	464	8	428.72	7.60	441.73	4.80
995	86.3	2778.5	440	10	460.64	4.69	476.54	8.30
994	86.8	2799.1	433	6	419.93	3.02	434.6	0.37
892	18.6	670	74	4	68.65	7.23	68.66	7.22
889	36.7	1320	224	10	242.27	8.16	242.47	8.25
861	50.2	1652	250	25	245.55	1.78	246.56	1.38
859	49.1	2741.2	97	5	92.06	5.09	93.29	3.82
					Avg.	5.37		4.88

[a] Hydrate as discontinuous phase.
[b] Liquid water as discontinuous phase.

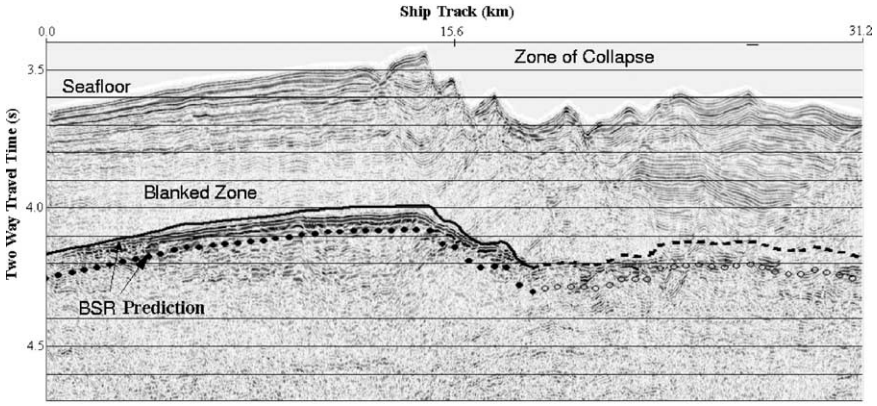

Fig. 5. Line 18 Ship Track Seismic Profile: the black line is the prediction using Eq. (6) with clay percent of 85.2 and the circles are the predictions assuming a bulk phase, both with a geothermal gradient of $T(z) = 276.71 + 0.0356z$ (K).

hydrate as a discontinuous phase, that is having a different pressure than in the bulk, and the other with liquid water as the discontinuous phase. Details of calculations for discontinuous liquid water can be found in Klauda and Sandler (2001). The variation between the results for different choices of the discontinuous phase is small, with both predictions having about 5% AAD from the observed values, and both leading to similar predictions for the maximum hydrate stability depths. The differences between the two predictions are largest for the more clayey (small pore) sediment. Because of the similarity of the results, the likely discontinuous phase cannot be determined from comparison with observed maximum depths of hydrate. However, in general, hydrates fill less than 10% of the pore space substantiating the assumption that the hydrate phase is not continuous with the bulk, and this is what will be used here.

Previous predictions for the maximum depth of hydrate stability for ODP Leg 164 were made by Henry et al. (1999), and these were systematically more than 100 m deeper than the observed BSR for site 995. Henry et al. (1999) assumed that the hydrate phase was discontinuous, and used a measured PSD for site 995 with an average radius of about 1000 Å (Clennell et al., 1999). However, from Eq. (9) we estimate that the average pore radius to be about 170 Å, which changes the depth of the predicted BSR to within 20 m of the observed value. We believe that the BSR overprediction of Henry et al. (1999) was due to use of an inaccurate PSD.

Fig. 5 shows a seismic profile of the seafloor along Line 18 near Leg 164 (Taylor, Dillon, Anton, & Danforth, 1999). In our predictions of hydrate stability (the BSR), we assumed that the geothermal gradient and sediment type are the average values of those reported for ODP sites 994, 995, and 997, and that the speed of sound in the sediment was the average value reported in the ODP Initial Report (Paull et al., 1996). The heavy black line in Fig. 5 is the predicted BSR using our porous fugacity-based model, and the circles are the predictions assuming bulk phase equilibrium (that is, assuming an infinite pore radius). From the seismic graph the measured BSR is shown as the first black line between the model predictions and is almost parallel to the irregular seafloor for the ship track distance of 0.5–18.5 km. The dashed lines or open circles are the predictions in areas for which there was no measured BSR. The region labeled Blanked Zone in the figure is an area of weak reflection amplitude assumed to be the zone where methane hydrate fills the pore space to an appreciable extent such that there is a cementation of the strata by the methane hydrate (Dillon, Hutchinson, & Drury, 1996).

A heat transfer analysis was preformed to estimate the subseafloor temperature profile at a ship track distance of greater than 14 km (Fig. 5). In a two-dimensional heat transfer analysis, we assumed a triangular shape of the peaks with a constant seawater temperature on both sides of the peaks, and a constant geothermal heat flux at the base of the triangle from the geothermal heat flux. From this analysis, the temperatures in these peaks were essentially constant and equal to the seafloor temperature. Therefore, for the ship track of greater than 14 km in Fig. 5, the predictions are almost equivalent to those if the peaks are removed from the seafloor. Using this analysis, the porous fugacity model follows the measured BSR closely with only a 3.3% AAD, while the bulk phase prediction is systematically below the measured BSR (generally by 70 m) resulting in a 13.3% AAD.

4.2. Regional predictions

Next, we have used our model to estimate potential gas hydrate reserves in the Mediterranean Sea, Black Sea, Gulf of Mexico, and Northern Indian Ocean. For the Mediterranean Sea, water temperature near the seafloor and at a sufficient depth for hydrate stability can vary from 12 to 14 °C (Antonov et al., 1998a); a constant average value of 13 °C was used without a significant loss of accuracy. Similar 1 °C variations from the mean were observed for the bottom water temperatures in the Black Sea and Gulf of Mexico. The thickness of the hydrate stability zone is shown in Fig. 6(a) and is reduced by half compared to predictions for a ocean floor temperature of 1.5 °C. As stated above, predictions for the hydrate thermodynamic stability zone were made for regions with only 0.4 wt% of organic carbon or greater.

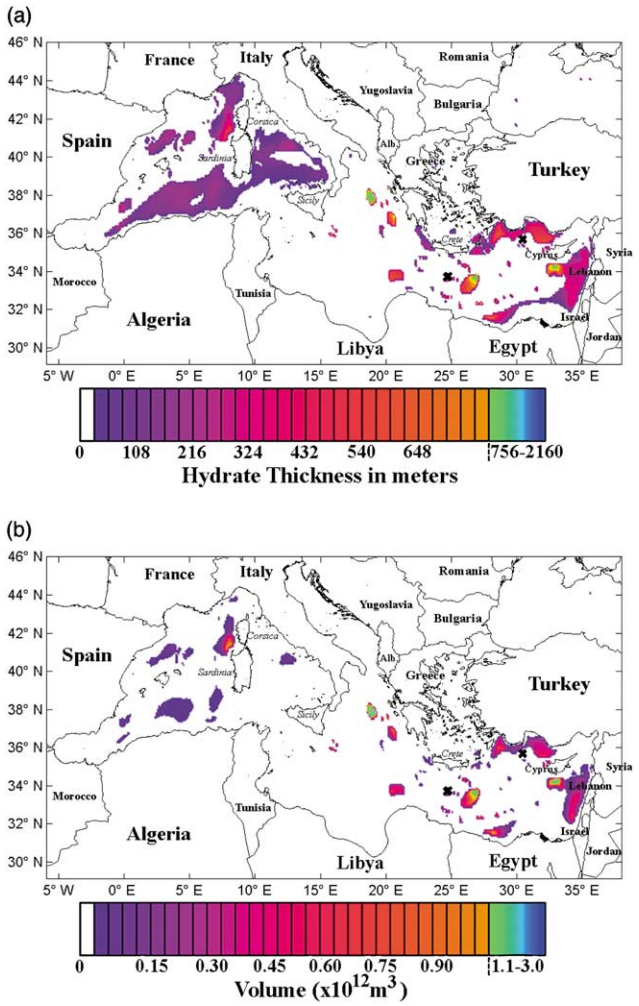

Fig. 6. Mediterranean Sea: (a) thickness of hydrate zone, (b) volume of methane in hydrate expanded to STP in a 0.1° Latitude by 0.1° Longitude area.

However, solving the set of mass transfer equations with a sedimentation rate of 12 cm kyr^{-1} (Romankevich, 1984) leads to negligible amounts of methane in some regions. For example, compare the western Mediterranean Sea areas in Fig. 6(a) that have hydrate stability zones ranging from 100 to 250 m thick with those same areas in Fig. 6(b) that are found to have little methane hydrate. This is largely a result of a relatively thin hydrate zone and only moderate levels of organic carbon, which results in a low hydrate saturation of the pore space. If the common assumption of a worldwide uniform hydrate filling of the pore space were used, those areas without hydrate in Fig. 6(b) but with the possible hydrate zone thicknesses shown in Fig. 6(a), would be incorrectly predicted to have hydrate. Therefore, accounting for methane transport is essential for accurate predictions for the amount of methane hydrate.

We predict that several areas in the Mediterranean Sea have significant amounts of gas hydrate: south of Cyprus, west of Greece, and off the western coast of the Corsica and Sardinia Islands. In these areas the conditions are favorable

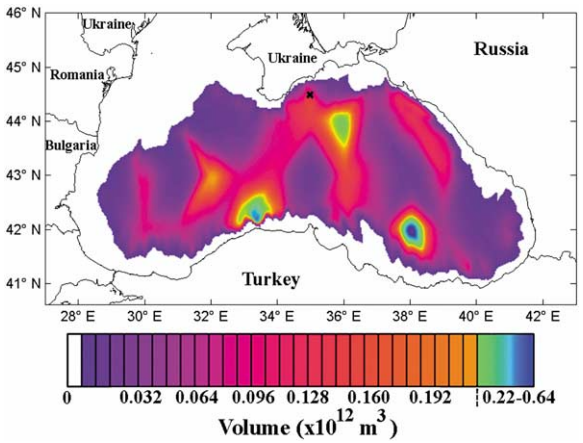

Fig. 7. Volume of methane in hydrate expanded to STP in a 0.05° Latitude by 0.05° Longitude area for the Black Sea.

due to a relatively high organic content in the sediment. Two samples of hydrate were recovered south of Crete near the region labeled with an **x** in Fig. 6, and this area is correctly predicted to be a hydrate-containing area using our model. However, our model does not predict hydrate at the observed location south of Turkey, as the amount of organic material is insufficient to produce methane from bacteria. Though it has been reported that this hydrate originates from a mud volcano, which is a region on the seafloor that episodically releases methane from deep sources and causes a nearby increase of seafloor temperature. To our knowledge, the locations of mud volcanoes and their methane fluxes cannot be predicted, and therefore our predictions do not include regions on the seafloor with mud volcanoes. Ignoring such sources of methane, the total amount of methane expanded to STP in the Mediterranean Sea is 0.59×10^{15} m^3.

We predict a relatively even distribution of methane in hydrated form in the Black Sea, with some local areas of high concentration as shown in Fig. 7. Here, a seafloor temperature of 9 °C (Antonov et al., 1998a) and an average

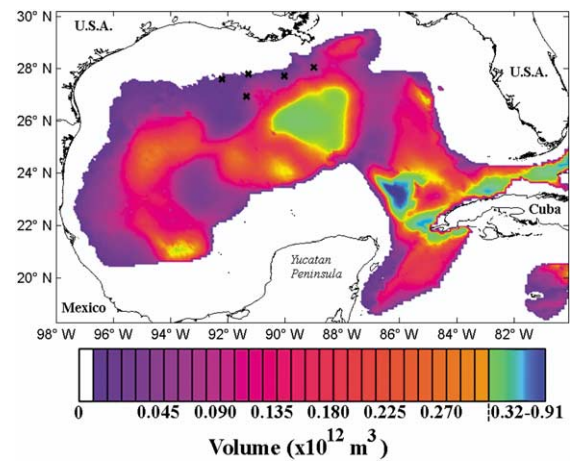

Fig. 8. Volume of methane in hydrate expanded to STP in a 0.1° Latitude by 0.1° Longitude area for the Gulf of Mexico.

sedimentation rate of 21 cm kyr^{-1} (Romankevich, 1984) were used in our predictions of hydrate volumes. Our model predicts the presence of hydrate in the observed location of a Black Sea hydrate (Kvenvolden & Loreson, 2001), though we estimate that the greatest amount of methane hydrate can be found in the southern Black Sea bordering Turkey. From our model we predict the amount of methane in hydrates expanded to STP in the Black Sea to be 0.85×10^{15} m^3.

The northwestern region of the Gulf of Mexico is known to have a widespread distribution of gas hydrates (Milkov & Sassen, 2001). From Fig. 8 all observed hydrate locations are correctly predicted by our model using a seafloor temperature of 4 °C taken from Antonov et al. (1998a) and a sedimentation rate of 13 cm kyr^{-1} (Romankevich, 1984). Previously Milkov and Sassen (2001) have estimated 0.012×10^{15} m^3 of methane expanded to STP for a region covering 59,000 km^2 in northwestern Gulf of Mexico, but we predict a methane reserve of 0.12×10^{15} m^3, an order of magnitude greater. Milkov and Sassen (2001) used a conservative value of 0.5% hydrate saturation of the pore space, but from our model the predicted average value is 5%, and this is the source of the discrepancy in the reserve estimates. Since we estimate hydrate saturation based on geologic variables rather than using ad hoc estimates, our predictions should be more accurate. Fig. 8 shows that the largest concentrations of methane hydrate are located in the center of the Gulf and northeast of the Yucatan Peninsula, with a total methane volume of 1.4×10^{15} m^3 for this region.

We predict that the Northern Indian Ocean (Arabian Sea and Bay of Bengal) has large concentrations of methane hydrate (Fig. 9). The seafloor temperature and sedimentation rate for this region was assumed to be constant at 1.5 °C and 10 cm kyr^{-1}, respectively. Bottom water temperatures can vary from 1 to 5 °C in the Northern Indian Ocean, but at depths below 2000 m where most of the hydrate is predicted by our model this range was reduced to 1–3 °C. Rao, Subrahmanyam, Rastogi, and Deka (2001) found that the highest concentrations of hydrates off the western coast of India occurred near Goa, on the central part of the Indian peninsula south of Bombay. Similarly, we predict potentially high volumes of methane in this region just east of the observed location in Fig. 9. However, the largest amount of methane hydrate is predicted to occur in the Arabian Sea offshore of Pakistan and Oman, and in the Bay of Bengal just south of Bangladesh. In these regions the high organic carbon content and moderately low seafloor porosity combine to result in high filling of the pore space by methane hydrate. For the region shown in Fig. 9 we predict that the total amount of methane in hydrate form when expanded to STP is 14.6×10^{15} m^3.

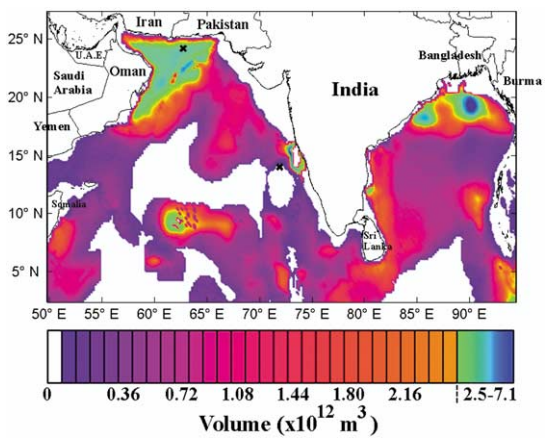

Fig. 9. Volume of methane in hydrate expanded to STP in a 0.2° Latitude by 0.2° Longitude area for Northern Indian Ocean.

5. Conclusions

Natural accumulations of methane hydrate in the seafloor depend on the conditions of thermodynamic stability and the mass transfer of methane. Hydrates are thermodynamically stable if the hydrostatic pressure is greater than the equilibrium pressure at a given sediment temperature. For accurate hydrate stability zone predictions the effect of pore size or sediment type should be included.

Although hydrates could be thermodynamically stable as a result of the sufficient hydrostatic pressure throughout most of the deep oceans, the availability of seafloor methane determines actual hydrate locations. In our model, based on methane production by bacteria from organic matter in the seafloor, we have found that 0.4% by weight of organic carbon is a reasonable estimate of the minimum amount required to produce significant amounts of methane. The amount of seafloor organic carbon interpolated from Premuzic et al. (1982) and Romankevich (1984) was used to determine the probable locations of methane hydrate.

Using this information and our fugacity-based model to determine hydrate zone thickness, the mass transfer equations of Davie and Buffett (2001) were solved to determine local amounts of methane hydrate for the Mediterranean Sea, Black Sea, Gulf of Mexico, and Northern Indian Ocean. Of the regions studied, our predictions show that the Arabian Sea potentially has large accumulations of methane hydrate, though the Gulf of Mexico and Black Sea also contain large methane reserves.

Although the focus of this research was to determine areas of hydrate occurrence, a similar approach could be used to determine locations in the ocean that could be used for the stable sequestering of carbon dioxide in the form of hydrate. Marine sediment injection of CO_2 within such zones of hydrate stability could reduce the amount of carbon dioxide released to the atmosphere as has been previously proposed. Such a study is currently underway.

Thermogenic and other deep sources of methane can also contribute to hydrate growth; one example is the observed hydrate near a mud volcano in the Mediterranean Sea. Although not included in our predictions, these sources of methane can produce hydrates that completely fill the pore space as a result of the high flux of methane (Milkov &

Sassen, 2002). Once estimates for their locations and fluid fluxes are available the mass transfer model Davie and Buffett (2001) can be used to estimate the amount of hydrates from these sources.

Acknowledgements

Financial support of this research was provided from contract DE-FG02-85ER13436 from the division of Basic Energy Sciences of the US Department of Energy and award number EEC 0085461 from the US National Science Foundation. The authors would wish to thank Drs. David N. Dewhurst and Andrew C. Aplin for sending us their experimental pore size distributions and William P. Dillon in supplying us with analyzed data from Taylor et al. (1999).

References

Antonov, J., Levitus, S., Boyer, T. P., Conkright, M., Brien, T. O., & Stephens, C. (1998a). *World Ocean Atlas 1998* (*Vol. 1*). *Temperature of the Atlantic Ocean*, Washington, DC: US Gov. Printing Office.

Antonov, J., Levitus, S., Boyer, T. P., Conkright, M., Brien, T. O., & Stephens, C. (1998b). *World Ocean Atlas 1998* (*Vol. 2*). *Temperature of the Pacific Ocean*, Washington, DC: US Gov. Printing Office.

Antonov, J., Levitus, S., Boyer, T. P., Conkright, M., Brien, T. O., Stephens, C., & Trotsenko, B. (1998c). *World Ocean Atlas 1998* (*Vol. 3*). *Temperature of the Indian Ocean*, Washington, DC: US Gov. Printing Office.

Behrmann, J. H., Lewis, S. D., Musgrave, R. J., Arqueros, R., Bangs, N. L., Boden, P., Brown, K. M., Collombat, H., Didenko, A. N., Didyk, B. M., Forsythe, R., Froelich, P. N., Golovchenko, X., Kumosov, V. B., Kvenvolden, K. A., Lindsly-Griffin, N., Marsaglia, K., Osozawa, S., Prior, D. J., Sawyer, D. S., Scholl, D. C., Spiegler, D., Strand, K., Takahashi, K., Torres, M. E., Faundez, M. V., Vergara, H. P., & Waseda, A. (1991). Sites 859, 860, and 861. *Proceedings of the Ocean Drilling Program, Initial Reports*, *141*, 1.

Brewer, P. G., Friederich, C., Peltzer, E. T., & Orr, F. M. (1999). Direct experiments on the ocean disposal of fossil fuel CO2. *Science*, *284*(5416), 943–945.

Brewer, P. G., Orr, F. M., Friederich, G., Kvenvolden, K. A., & Orange, D. L. (1998). Gas hydrate formation in the deep sea: In situ experiments with controlled release of methane, natural gas, and carbon dioxide. *Energy and Fuels*, *12*(1), 183–188.

Brown, K. M., Bangs, N. L., Froelich, P. N., & Kvenvolden, K. A. (1996). The nature, distribution, and origin of gas hydrate in the Chile Triple Junction region. *Earth and Planetary Science Letters*, *139*(3–4), 471–483.

Clarke, M. A., Pooladi-Darvish, M., & Bishnoi, P. R. (1999). A method to predict equilibrium conditions of gas hydrate formation in porous media. *Industrial and Engineering Chemistry Research*, *38*(6), 2485–2490.

Clennell, M. B., Hovland, M., Booth, J. S., Henry, P., & Winters, W. J. (1999). Formation of natural gas hydrates in marine sediments 1. Conceptual model of gas hydrate growth conditioned by host sediment properties. *Journal of Geophysical Research-Solid Earth*, *104*(B10), 22985–23003.

Cramer, S. D. (1984). Solubility of methane in brines from 0-Degrees-C to 300-Degrees-C. *Industrial and Engineering Chemistry Process Design and Development*, *23*(3), 533–538.

Davie, M. K., & Buffett, B. A. (2001). A numerical model for the formation of gas hydrate below the seafloor. *Journal of Geophysical Research-Solid Earth*, *106*(B1), 497–514.

Dewhurst, D. N., Aplin, A. C., & Sarda, J. P. (1999). Influence of clay fraction on pore-scale properties and hydraulic conductivity of experimentally compacted mudstones. *Journal of Geophysical Research-Solid Earth*, *104*(B12), 29261–29274.

Dewhurst, D. N., Aplin, A. C., Sarda, J. P., & Yang, Y. L. (1998). Compaction-driven evolution of porosity and permeability in natural mudstones: An experimental study. *Journal of Geophysical Research-Solid Earth*, *103*(B1), 651–661.

Dillon, W. P., Hutchinson, D. R., & Drury, R. M. (1996). Seismic reflection profiles on the Blake Ridge near Sites 994, 995, and 997. *Proceedings of the Ocean Drilling Program, Initial Reports*, *164*, 47–56.

Gornitz, V., & Fung, I. (1994). Potential distribution of methane hydrates in the worlds oceans. *Global Biogeochemical Cycles*, *8*(3), 335–347.

Gosnold, W. D. (2001). *The global heat flow database*. International Heat Flow Commission.

Handa, Y. P., & Stupin, D. (1992). Thermodynamic properties and dissociation characteristics of methane and propane hydrates in 70-Angstrom-radius silica-gel pores. *Journal of Physical Chemistry*, *96*(21), 8599–8603.

Hatzikiriakos, S. G., & Englezos, P. (1993). The relationship between global warming and methane gas hydrates in the earth. *Chemical Engineering Science*, *48*(23), 3963–3969.

Hatzikiriakos, S. G., & Englezos, P. (1994). Permafrost melting and stability of offshore methane hydrates subject to global warming. *International Journal of Offshore and Polar Engineering*, *4*(2), 162–166.

Henry, P., Thomas, M., & Clennell, M. B. (1999). Formation of natural gas hydrates in marine sediments 2. Thermodynamic calculations of stability conditions in porous sediments. *Journal of Geophysical Research-Solid Earth*, *104*(B10), 23005–23022.

Holbrook, W. S., Hoskins, H., Wood, W. T., Stephen, R. A., & Lizarralde, D. (1996). Methane hydrate and free gas on the Blake Ridge from vertical seismic profiling. *Science*, *273*(5283), 1840–1843.

Klauda, J. B., & Sandler, S. I. (2000). A fugacity model for gas hydrate phase equilibria. *Industrial and Engineering Chemistry Research*, *39*(9), 3377–3386.

Klauda, J. B., & Sandler, S. I. (2001). Modeling gas hydrate phase equilibria in laboratory and natural porous media. *Industrial and Engineering Chemistry Research*, *40*(20), 4197–4208.

Kvenvolden, K. A., & Grantz, A. (1990). *Gas hydrates of Arctic Ocean, The Arctic Ocean Region*. Boulder: Geological Society of America, pp. 539–549.

Kvenvolden, K. A., & Loreson, T. D. (2001). A global inventory of natural gas hydrate occurrence. *USGS: Western Region Coastal and Marine*.

Lide, D. R., & Frederiskse, H. P. R. (1995). *CRC handbook*. Boca Raton, FL: CRC Press.

MacDonald, G. (1990). Role of methane clathrates in past and future climates. *Climatic Change*, *16*, 247–281.

Milkov, A. V., & Sassen, R. (2001). Estimate of gas hydrate resource, northwestern Gulf of Mexico continental slope. *Marine Geology*, *179*(1–2), 71–83.

Milkov, A. V., & Sassen, R. (2002). Economic geology of offshore gas hydrate accumulations and provinces. *Marine and Petroleum Geology*, *19*(1), 1–11.

Miller, M., Smith, W. H. F., Kuhn, J., & Sandwell, D. T. (2000). *An interactive global map of sea floor topography based on satellite altimetry and ship depth soundings*. NOAA Laboratory for Satellite Altimetry.

Musich, L., Bearman, S., Birtley, T., Hawkins, D., Long, B., Marsee, D., Pinkston, B., Wood, T., & Woodbury, P. (2000). *Core data from the deep sea drilling project*. Boulder: World Data Center for Marine Geology and Geophysics.

Parrish, W. R., & Prausnitz, J. M. (1972). Dissociation pressures of gas hydrates formed by gas mixtures. *Industrial Engineering and Chemistry Design and Developement*, *11*(1), 26–35.

Patwardhan, V. S., & Kumar, A. (1986). A unified approach for prediction of thermodynamic properties of aqueous mixed-electrolyte solutions 1. Vapor-pressure and heat of vaporization. *AIChE Journal*, *32*(9), 1419–1428.

Paull, C. K., Matsumoto, R., Wallace, P. J., Black, N. R., Borowski, W. S., Collett, T. S., Damuth, J. E., Dickens, G. R., Egeberg, P. K., Goodman, K., Hesse, R. F., Hiroki, Y., Holbrook, S. W., Hoskins, H., Ladd, J., Lodolo, E., Loreson, T. D., Musgrave, R. J., Nahr, T., Okada, H., Pierre, C., Ruppel, C., Satoh, M., Thiery, R., Watanabe, Y., Wehner, H., Winters, W. J., & Wood, W. T. (1996). Sites 994, 995, and 996. *Proceedings of the Ocean Drilling Program, Initial Reports*, *164*, 99.

Pitzer, K. S., & Mayorga, G. (1973). Thermodynamics of electrolytes. II. Activity and osmotic coefficients for strong electrolytes with one or both ions univalent. *Journal of Physical Chemistry*, *77*(19), 2300–2308.

Pollack, H. N., Hurter, S. J., & Johnson, J. R. (1993). Heat flow from the Earth's interior: Analysis of the global data set. *Reviews of Geophysics*, *31*(3), 267–280.

Premuzic, E. T., Benkovitz, C. M., Gaffney, J. S., & Walsh, J. J. (1982). The nature and distribution of organic matter in surface sediments of world oceans and seas. *Organic Geochemistry*, *4*, 63–77.

Rao, Y. H., Subrahmanyam, C., Rastogi, A., & Deka, B. (2001). Anomalous seismic reflections related to gas/gas hydrate occurrences along the western continental margin of India. *Geo-Marine Letters*, *21*(1), 1–8.

Revelle, R. R. (1983). Methane hydrates in continental slope sediments and increasing atmospheric carbon dioxide, changing climate. *Report of the Carbon Dioxide Assessment Committee*. Washington, DC: National Academic Press, pp. 252–261.

Romankevich, E. A. (1984). *Geochemistry of organic matter in the ocean*. Berlin: Springer.

Ruppel, C. (1997). Anomalously cold temperatures observed at the base of the gas hydrate stability zone on the US Atlantic passive margin. *Geology*, *25*(8), 699–702.

Sloan, E. D. (1998). *Clathrate hydrates of natural gases*. New York: Marcel Dekker.

Smith, W. H. F., & Sandwell, D. T. (1997). Global sea floor topography from satellite altimetry and ship depth soundings. *Science*, *277*(5334), 1956–1962.

Taylor, M. H., Dillon, W. P., Anton, C. H., & Danforth, W. (1999). Seismic-reflection surveys of the Blake Ridge, R/V Cape Hatteras 1992 and 1995: Data acquisition, navigation and processing. *USGS. Open File Report*, 99–372.

Uchida, T., Ebinuma, T., & Ishizaki, T. (1999). Dissociation condition measurements of methane hydrate in confined small pores of porous glass. *Journal of Physical Chemistry B*, *103*(18), 3659–3662.

van der Waals, J. H., & Platteeuw, J. C. (1959). Clathrate solutions. *Advances in Chemical Physics*, *2*, 1.

Westbrook, G. K., Carson, B., Musgrave, R. J., Ashi, J., Baranov, B. V., Brown, K. M., Camerlenghi, A., Caulet, J.-P., Chamov, N., Ben Clennell, M., Cragg, B. A., Dietrich, P., Foucher, J.-P., Housen, B., Hovland, M., Jarrard, R. D., Kastner, M., Kopf, A., MacKay, M. E., Moore, C., Moran, K., Parkes, R. J., Sample, J., Sato, T., Screaton, E. J., Tobin, H. J., Whiticar, M. J., & Zellers, S. D. (1994). Sites 889, 890, and 892. *Proceedings of the Ocean Drilling Program, Initial Reports*, *146*, 127.